Zhou et al., http://www.jcb.org/cgi/content/full/jcb.201605101/DC1

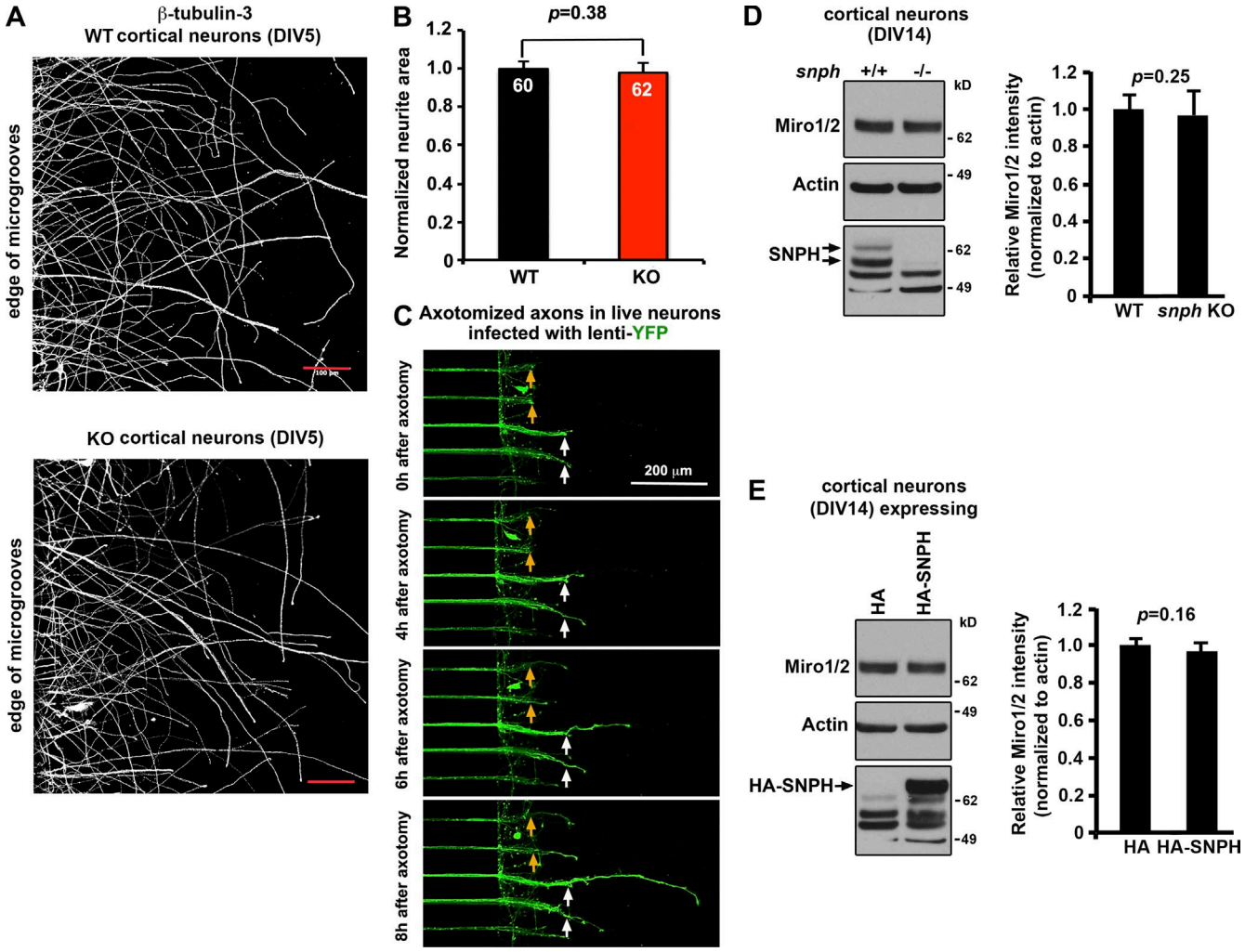

Figure S1. **Deleting *snph* does not change early axonal growth, and Miro1/2 expression is not regulated by SNPH.** (A and B) Representative images (A) and quantitative analysis (B) showing no observable change in early axonal growth of *snph* KO neurons before axotomy. WT and *snph* KO cortical neurons grown on microfluidic chambers were immunostained with βIII-tubulin at DIV5. Note that the normalized axonal area grown from each microgroove was not significantly altered between WT and *snph* KO neurons (P = 0.38). (C) Representative time-lapse images of live neurons showing regenerating axons from the axotomized tips. The *snph* KO cortical neurons were infected with lenti-YFP and axotomized in axonal terminal chambers at DIV10. Time-lapse images were captured at 0, 4, 6, and 8 h after axotomy. White and yellow arrows point to axotomized sites. Data were collected from the total number of microgrooves shown in the bars and expressed as mean ± SE and statistically analyzed by paired Student's *t* test. Bars: (A) 100 µm; (C) 200 µm. (D and E) Representative immunoblots and quantitative analysis showing that cortical neurons (DIV14) deleting *snph* (D) or overexpressing SNPH (E) display no detectable change in Miro1/2 expression. WT cortical neurons were infected by lentivirus HA-SNPH or HA control, and then Miro1/2 expression was examined at DIV14. Equal amounts (20 µg) of cell lysates from cultured neurons were loaded and sequentially immunoblotted with antibodies on the same membranes after stripping between applications of each antibody. Note that the *snph* KO or WT neurons overexpressing HA-SNPH do not change Miro1/2 expression. The relative intensity of Miro1/2 was quantified from three repeats and normalized to actin. Data are expressed as mean ± SE and statistically analyzed by paired Student's *t* test.

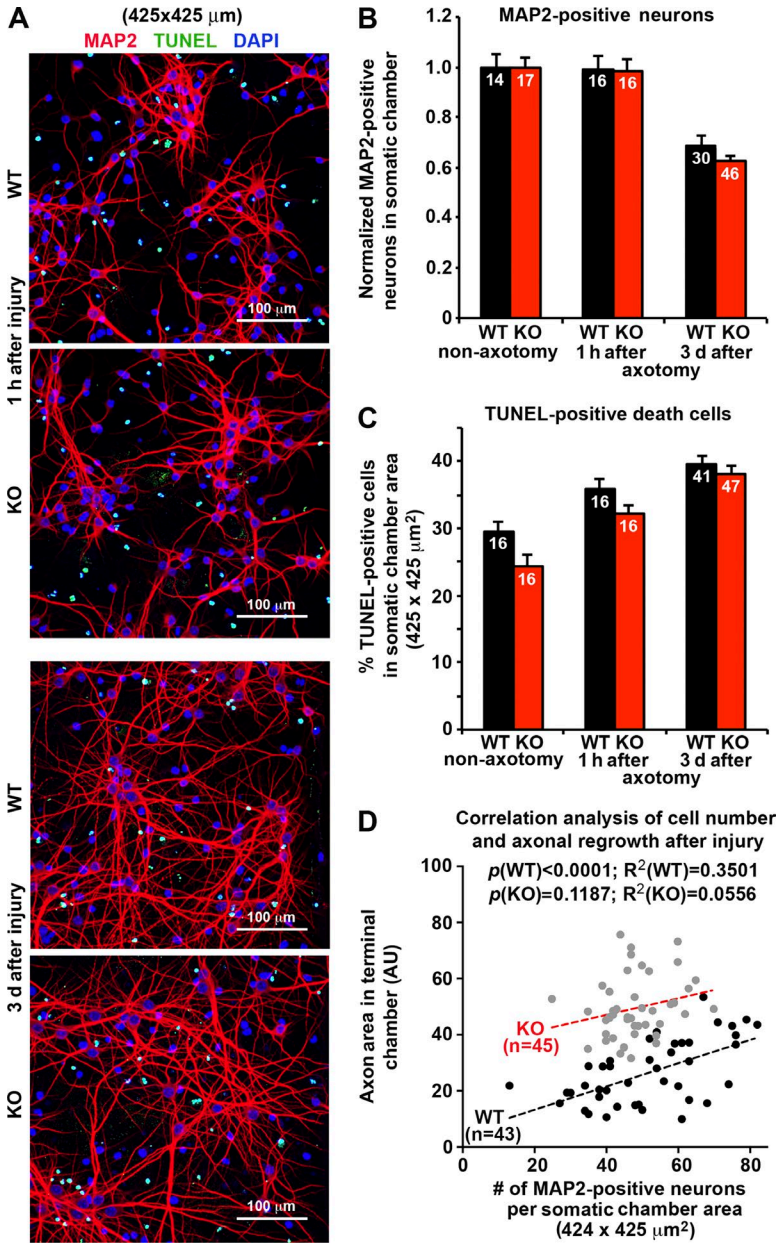

Figure S2. **Enhanced axonal regrowth in *snph* KO neurons is not directly correlated with cell density in the somatic chambers.** (A–C) Representative images (A) and quantitative analysis showing normalized MAP2-positive neurons (B) and the percentage of TUNEL-positive death cells (C) in the somatic chambers. 0.2×10^6 (10^7/ml) E18 mouse cortical neurons were plated in the somatic chamber, and axotomy was performed at DIV7 in the axonal terminal chamber. The number of MAP2-labeled neurons in the somatic chamber was counted before and 1 h and 3 d after axotomy, and data were normalized to that from neurons before axotomy. The percentage of TUNEL-positive cells to total DAPI staining in each somatic image field was calculated based on automatic watershed binary images. Note that no significant change was observed in the normalized density of MAP2-positive neurons and the percentage of TUNEL-positive death cells between WT and *snph* KO neurons at 1 h and 3 d after axotomy ($P > 0.05$). (D) Relative correlation between neuron density and axonal regrowth after injury. Although WT soma density correlates with axonal regrowth after injury ($R^2 = 0.3501$, $P < 0.0001$), enhanced axonal regrowth in *snph* KO neurons is not directly correlated with relative neuron density in the somatic chamber ($R^2 = 0.0556$, $P = 0.1187$). Data were collected from the total number of images (425 × 425 μm²) shown in the bars and are expressed as mean ± SE and analyzed by one-way ANOVA, Kruskal–Wallis test.

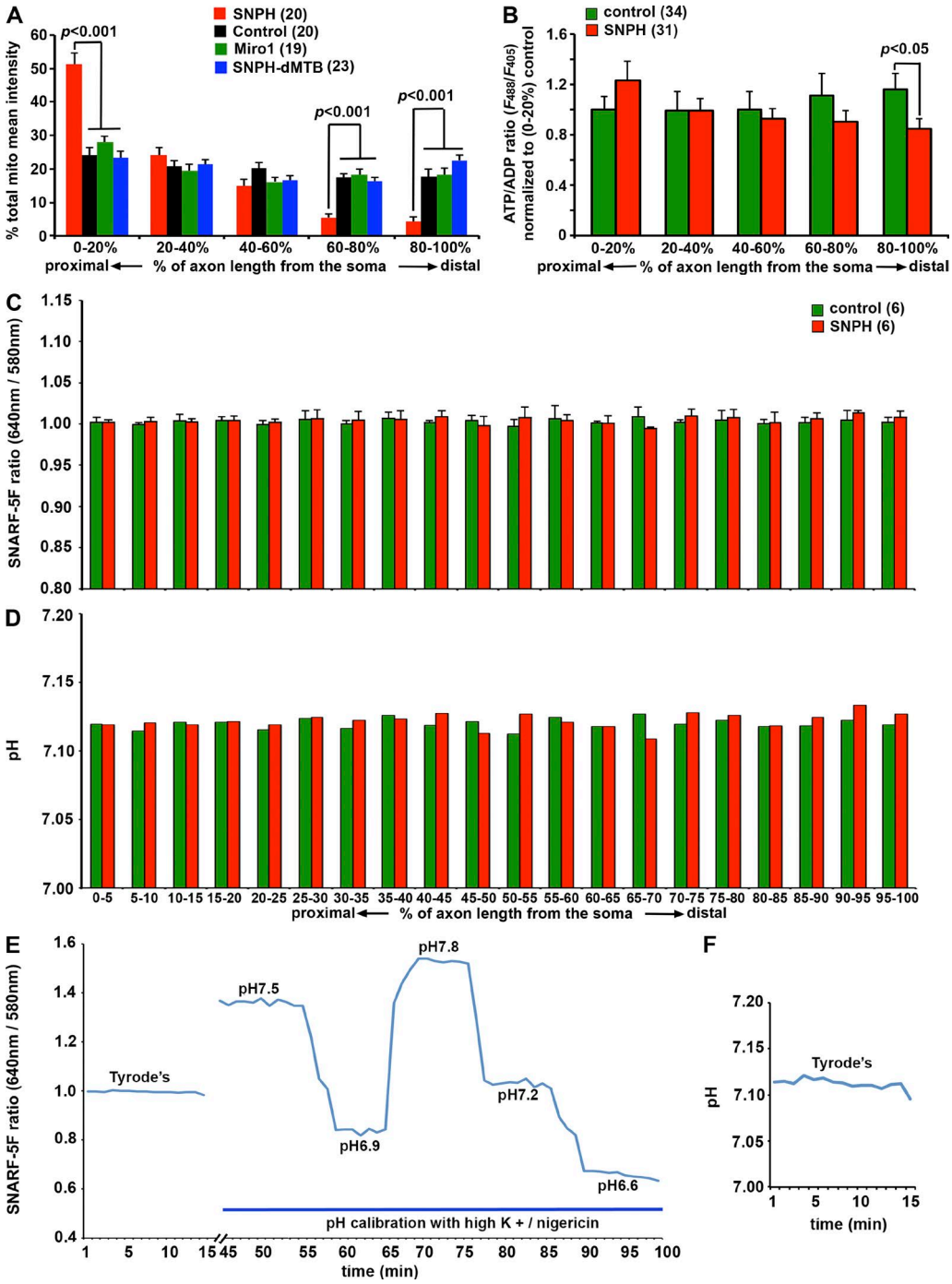

Figure S3. **Overexpressing SNPH alters mitochondrial distribution and ATP/ADP ratio in distal axons.** (A) Quantitative analysis showing relative mitochondrial distribution along an entire axon of cortical neurons coexpressing DsRed-Mito with GFP or together with SNPH, SNPH-dMTB, or Miro1. Neurons at DIV5 were immunostained with Tau. (B) Quantitative analysis showing relative cellular ATP/ADP ratio along an entire axon of cortical neurons coexpressing DsRed-Mito with GFP or SNPH. The cellular ATP/ADP ratio was measured by applying an engineered fluorescent ATP sensor PercevalHR in live neurons. The fluorescence intensity ratio (F_{488nm}/F_{405nm}) of Perceval reflects the relative ATP/ADP ratio. Relative mitochondrial distribution and ATP/ADP ratios along an axon were analyzed based on five equally divided segments (20%) of each individual axon from the most proximal to the most distal region. Note that overexpressing SNPH in cortical neurons redistributes mitochondria to the proximal region ($P < 0.001$), thus reducing mitochondrial density and ATP/ADP ratio in the most distal axon segment ($P < 0.001$ and $P < 0.05$, respectively). (C and D) Measurement of axonal pH using the pH dye SNARF-5F. Axonal pH was analyzed based on 20 equally divided segments (5%) of each axon from the most proximal to the most distal region. SNARF-5F was excited at 488 nm and detected around 580 and 640 nm. The ratio (640/580 nm; C) and calibrated pH value (D) were calculated at each 5% segment of axons as indicated. Calibrated pH values were averaged from a total of six axons. Note that pH values in an entire axon of both WT and SNPH-overexpressing neurons undergo very minor changes (7.10–7.15). Thus, reduction in the ATP/ADP ratios in distal axons expressing SNPH is physiologically relevant to reduced axonal mitochondrial density. (E and F) SNARF-5F signal was calibrated using various buffered solutions containing high K^+/nigericin with varying pH values. Axons were imaged in Tyrode's solution for 15 min, followed by a 30-min incubation in high K^+/nigericin, pH 7.5, solution. Then the SNARF-5F signal was calibrated by varying pH solutions. Images were taken once per minute. Data were analyzed from the total number of axons indicated in parentheses from three experiments and expressed as mean ± SE and by one-way ANOVA test.

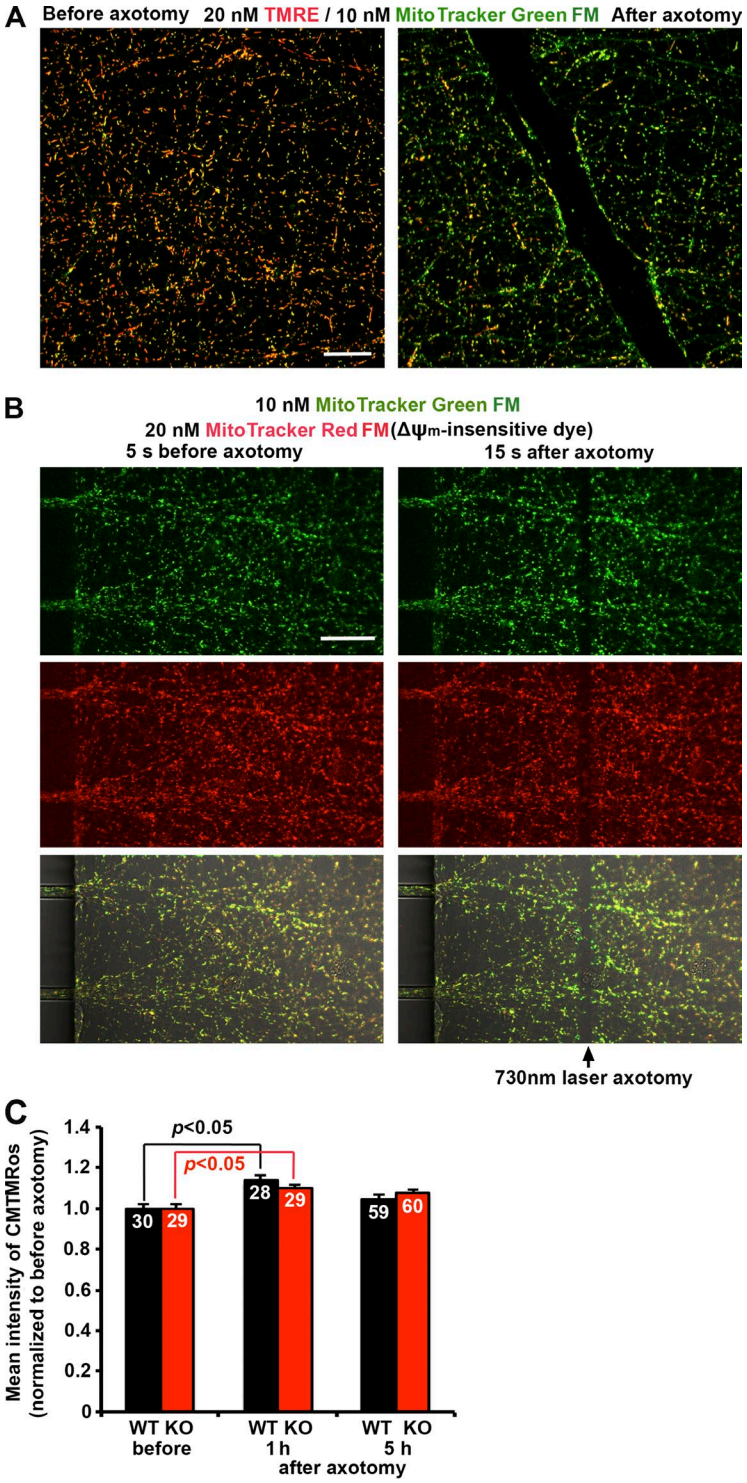

Figure S4. **Axotomy stress induces mitochondrial depolarization.** (A) Representative images showing physical axotomy-induced mitochondrial depolarization. A physical axotomy was applied in the axonal chamber by using pulled glass capillaries (World Precision Instruments) with a tip diameter of ∼1 µm that were prepared from Sutter Instrument (p-97). Neurons at DIV10 were loaded with 20 nM TMRE ($\Delta\psi_m$-dependent dye) and 10 nM MitoTracker Green FM ($\Delta\psi_m$-independent dye) before axotomy. The same image field was taken showing mitochondrial $\Delta\psi_m$ before and after physical axotomy. Note that after a physical axotomy, TMRE staining of mitochondria is lost near the axotomized ends, whereas MitoTracker Green FM staining remains. (B) Representative images showing that laser axotomy does not reduce the signal intensity of MitoTracker Red FM. The axonal chambers were loaded with 10 nM MitoTracker Green FM and 20 nM MitoTracker Red FM ($\Delta\psi_m$-insensitive dye with similar wavelength as TMRE). A 730-nm laser-induced axotomy was applied in the axonal chamber. The same image field was taken showing mitochondria at 5 s before and 15 s after laser axotomy. Note that laser axotomy does not reduce signal intensity of MitoTracker Red FM, thus excluding an artificial effect of 730-nm laser on TMRE signals with the similar wavelength. (C) Quantitative analysis showing that somatic mitochondria maintain $\Delta\psi_m$ after axotomy. Somatic mitochondrial integrity was examined by loading MitoTracker Orange-CMTMRos, a fixable $\Delta\psi_m$-dependent dye, before and 1 and 5 h after injury in WT and KO cortical neurons. Note that there is a subtle increase in the mean intensity of Orange-CMTMRos at 1 h after injury in both WT and KO neurons. Data were collected from the total number of images (425 × 425 µm^2) shown in the bars and are expressed as mean ± SE and analyzed by one-way ANOVA, Kruskal–Wallis test. Bars, 100 µm.

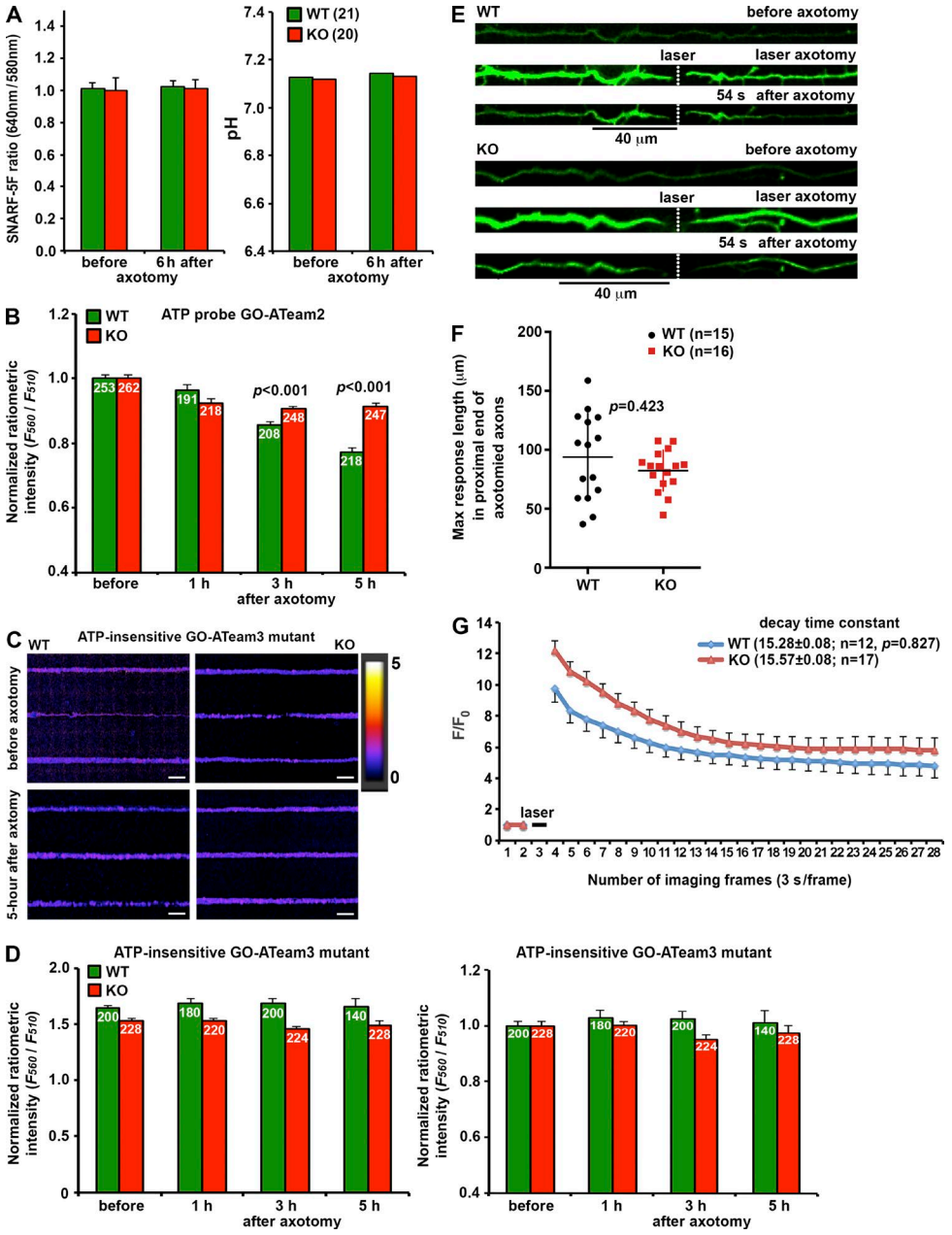

Figure S5. **Energy deficit recovery and calcium buffering in *snph* KO neurons after axotomy.** (A) Measurement of pH at regrowing axonal tips using the pH dye SNARF-5F. SNARF-5F was excited at 488 nm and detected at 580 and 640 nm. The ratio (640/580 nm) was calculated from regrowing axons 6 h after axotomy, and relative pH was calibrated on SNARF-5F signal with various buffered solutions containing high K/nigericin with varying pH values (also see Fig. S3 E). Note that axon terminal pH values in both WT and *snph* KO neurons undergo very minor changes (7.10–7.15). Data were analyzed from the total number of axon terminals indicated in parentheses from three experiments and expressed as mean ± SE and by one-way ANOVA test. (B) Normalized F_{560nm}/F_{510nm} ratiometric integrated intensity of ATP probe GO-ATeam2 and ATP-insensitive GO-ATeam3 mutant (R122K/R126K). Both WT and *snph* KO cortical neurons were transfected with ATP-sensitive GO-ATeam2 probe or ATP-insensitive GO-ATeam3 mutant, followed by imaging along microgrooves before or 1, 3, or 5 h after axotomy. F_{560nm}/F_{510nm} ratiometric integrated intensity was normalized to the ratiometric intensity before axotomy. Data were analyzed from the total number of microgrooves indicated within bars and expressed as mean ± SE and Student's *t* test. (C and D) Pseudo-color ratiometric images (C) and the F_{560nm}/F_{510nm} ratiometric intensity (D) of ATP-insensitive GO-ATeam3 mutant (R122K/R126K). Both WT and *snph* KO cortical neurons were transfected with ATP-insensitive GO-ATeam3 mutant, followed by imaging distal 150-μm microgrooves before or 1, 3, or 5 h after axotomy. Note that WT neurons expressing ATP-insensitive GO-ATeam3 mutant do not show a significant change in the F_{560nm}/F_{510nm} ratiometric intensity after axotomy. Data were analyzed from the total number of microgrooves indicated within bars and expressed as mean ± SE and Student's *t* test. Bars, 20 μm. (E–G) Representative images (E) and quantitative analysis (F and G) showing similar axotomy-induced Ca^{2+} waveform between adult WT and KO DRG neurons. The green fluorescent Ca^{2+} sensor G-GECO1.2 (K_d = 1.15 μM; Di Giovanni and Sheng, 2015) was electroporated into adult DRG neurons at DIV0 and imaged 2 d later. The multi-timer macro was applied for consecutive laser axotomy and image acquiring (E). In brief, after two frames of baseline acquisition, two-photo laser 730 was applied at the third frame, and then another 26 frames were collected at 512 × 512–pixel resolution (12 bit) with 3-s intervals. The white dotted lines (E) or black bar (G) indicates laser-induced axotomy. Note that the maximal distance of Ca^{2+} sensor response was unchanged after deleting *snph* (P = 0.423; F), and the mean decay time constant within 40 μm of the proximal end of injured axons (black bars under images), calculated based on fluorescent intensity (F/F_0) curve with a nonlinear fit, was not significantly changed (WT: 15.28 ± 0.08, KO: 15.57 ± 0.08, P = 0.827; G). Data are expressed as mean ± SE and were statistically analyzed by Mann–Whitney *U* test.

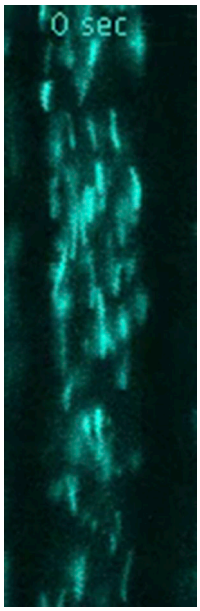

Video 1. **Ex vivo imaging of axonal mitochondrial transport along the sciatic nerve in Thy1-Mito-CFP mice.** Mitochondrial transport was assessed in sciatic nerve explants after rapid dissection and immediate immersion in prewarmed oxygenated Neurobasal-A medium. Time-lapse images of multiple axons in nerve explants were acquired using an LSM 510 META confocal microscope (ZEISS) with a P-Apochromat 40×/1.3 oil objective at 3-s intervals for a total of 100 frames. Image stacks were processed using the free ImageJ software v1.43 and associated plugins.

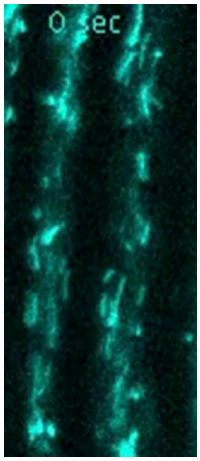

Video 2. **Ex vivo imaging of axonal mitochondrial transport along the sciatic nerve in the crossed *snph* KO/Thy1-Mito-CFP mice.** Thy1-Mito-CFP transgenic mice were crossed with C57BL/6 background *snph*$^{-/-}$ mice to generate *snph* KO/Mito-CFP mice. Mitochondrial transport was assessed in sciatic nerve explants from the crossed *snph* KO/Mito-CFP mice. The sciatic nerve was dissected rapidly and immediately immersed in prewarmed oxygenated Neurobasal-A medium. Time-lapse images of multiple axons in nerve explants were acquired using an LSM 510 META confocal microscope (ZEISS) with a P-Apochromat 40×/1.3 oil objective at 3-s intervals for a total of 100 frames. Image stacks were processed using the free ImageJ software v1.43 and associated plugins. Note that deleting *snph* robustly enhances axonal mitochondrial transport along axonal bundles of sciatic nerve.

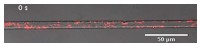

Video 3. **Axonal mitochondrial motility along microgrooves from cortical neurons overexpressing SNPH.** Cortical neurons were infected with lentivirus coexpressing DsRed-Mito and SNPH. Isolated axon bundles in the microgrooves were selected for time-lapse imaging at DIV12. Time-lapse sequences were collected at 5-s intervals for a total of 100 frames. Note that expressing SNPH abolishes mitochondrial transport in axons. Left side is toward the somatic chamber.

Video 4. **Axonal mitochondrial motility along microgrooves from cortical neurons overexpressing SNPH-dMTB.** Cortical neurons were infected with lentivirus coexpressing DsRed-Mito and SNPH-dMTB. Isolated axon bundles in the microgrooves were selected for time-lapse imaging at DIV12. Time-lapse sequences were collected at 5-s intervals for a total of 100 frames. Left side is toward the somatic chamber.

Video 5. **Axonal mitochondrial motility along microgrooves from cortical neurons overexpressing Miro1.** Cortical neurons were infected with lentivirus coexpressing DsRed-Mito and Miro1. Isolated axon bundles in the microgrooves were selected for time-lapse imaging at DIV12. Time-lapse sequences were collected at 5-s intervals for a total of 100 frames. Note that expressing Miro1 enhances mitochondrial transport in axons. Left side is toward the somatic chamber.

Video 6. **Axotomy stress depolarizes mitochondria in the vicinity of injured sites.** Mature cortical neurons grown on microfluidic chambers were infected with pLenti-GFP. Axons in the terminal chambers were loaded with 25 nM TMRE dye at DIV12, followed by laser axotomy and time-lapse imaging. In brief, for real-time image capture of laser axotomy, both acquisition and bleach setting were reused in separate blocks. The images were first recorded at 5-s intervals for a total of 50 frames, and then the 730-nm laser was powered-up with 70% output and pixel dwell time >20 µs in cropped imaging region for bleaching. The consecutive post-axotomy recording was collected at 5-s intervals for a total of 100 frames. For a successful laser axotomy, the axons in the DIC image were observed with a structural break down or invasion of extracellular dye. Note that GFP-labeled axons are quickly broken up upon axotomy (left) and mitochondria in the vicinity suddenly lose their TMRE staining (right).

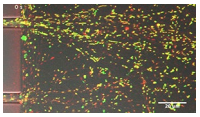

Video 7. **Axotomy stress depolarizes mitochondria in the vicinity of injured sites.** Neurons were infected with pLenti-GFP-Mito, and axon bundles in the terminal chambers were loaded with 25 nM TMRE dye at DIV12. Laser axotomy and time-lapse imaging were used to acquire axon bundles with a 40× lens. The images were first recorded at 5-s intervals for a total of 50 frames; then the 730-nm laser was powered-up with 70% output and pixel dwell time >20 µs in the cropped imaging region for bleaching. The consecutive post-axotomy recording was collected at 5-s intervals for a total of 50 frames. Note that axotomy triggers a sudden loss of mitochondria staining by TMRE near the injured site, whereas those depolarized mitochondria maintain their GFP-Mito signals, and thus the color of mitochondria was switched from yellow (healthy) to green (depolarized).

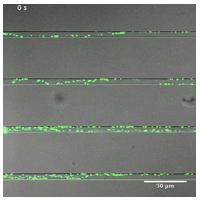

Video 8. **Axonal mitochondrial motility along microgrooves from WT cortical neurons 1 h after axotomy.** Neurons were infected with pLenti-GFP-Mito. Time-lapse images were acquired in isolated axon bundles with a 40× lens and recorded for a total of 100 frames at 5-s intervals. Left side is toward the somatic chamber.

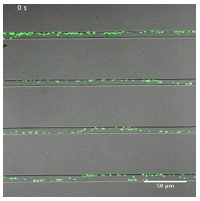

Video 9. **Enhanced mitochondrial motility along microgrooves from *snph* KO cortical neurons 1 h after axotomy.** Neurons were infected with pLenti-GFP-Mito. Time-lapse images were acquired in isolated axon bundles with a 40× lens for a total of 100 frames at 5-s intervals. Note that deleting *snph* significantly enhances axonal mitochondrial transport. Left side is toward the somatic chamber.

Reference

Di Giovanni, J., and Z.H. Sheng. 2015. Regulation of synaptic activity by snapin-mediated endolysosomal transport and sorting. *EMBO J.* 34:2059–2077. http://dx.doi.org/10.15252/embj.201591125